International Journal of Environmental Sciences
ISSN: 2229-7359
Vol. 11 No. 11s, 2025
https://theaspd.com/index.php

Green Synthesis Of Silver Nanoparticles Using N-Acetyl- L - Cysteine For Colorimetric Detection Of Methamphetamine

Jumana M. Al-Rikabi[1*], Zainab Shakir Abdullah Al-Ali[2], Ibrahim M. Al-Naiema[3]
[1,2,3]Department of Chemistry, College of Science, University of Basrah, Basrah, Iraq.
*jumana.khalaf@stu.edu.iq
Received:08-05-2025 Accepted:21-06-2025 Published: 22-06-2025

Abstract

Methamphetamine (METH) addiction has become a serious public health problem, worldwide. In this study, an alternative eco-friendly method for the synthesis of silver nanoparticles (AgNPs) using N-acetyl-L-cysteine (NAC) as a reducing and stabilizing agent was proposed. The biosynthesized AgNPs were conjugated with a specific aptamer to develop a label-free colorimetric sensor for the highly sensitive and selective quantification of METH. The prepared nanoparticles were characterized using UV-Vis, FTIR, XRD, TEM, FE-SEM, EDX, DLS and Zeta potential measurements. The results indicated that silver nanoparticles were successfully prepared (15-25 nm), and they were stable and homogeneous. The colorimetric sensing platform showed with the naked eye a color change upon detection of METH, which was caused by the aggregation of the nanoparticles induced by aptamer-target binding offering a visual and spectrophotometric read-out. The biosensor presented in this work provides an inexpensive, rapid and non-invasive method for determining the presence of methamphetamine. Thus, the outcomes of this study can be vastly utilized in forensic and clinical applications.

1. INTRODUCTION

Methamphetamine (METH) is a psychostimulant that is widely abused across the globe, and it is the second most illicitly abused drug after marijuana [1]. METH is an addictive central nervous system stimulant with cardiovascular, hyperthermic, and anorexigenic actions. Some of the neurological and psychiatric effects of METH are cerebrovascular accidents, convulsions, schizophrenia and other psychotic disorders [2–6]. Methamphetamine abuse has increased markedly over the past years and has become a serious social and health problem in Iraq. This epidemic is particularly prominent in Basra city, where the illicit use of methamphetamine and Captagon has significantly increased[7,8]. Its ready availability, especially among youth, has resulted in significant health problems and increased suicidal ideation [9]. Therefore, it is crucial to provide an easy and readily available means to detect and quantify METH in biological samples. Several techniques have been used for the quantitative analysis of METH in blood, hair, plasma, urine, saliva, and nails such as gas–chromatography-mass spectrometry (GC-MS), high-performance liquid chromatography (HPLC), liquid chromatography-mass spectrometry (LC-MS), ion mobility spectrometry (IMS), capillary electrophoresis (CE), immunoassays, etc[10]. However, these methods still have the disadvantages of expensive instruments, time-consuming process, environmental pollution or lack of specificity, although they have shown acceptable sensitivity [11–13]. As such, the development of new probes and sensors for the highly sensitive and selective detection of METH is greatly needed.Colorimetric sensors, reporting detection of target analytes by exhibiting a visible-color change in the reaction medium have been highly accepted as simple, user-friendly, and efficient means of METH detection [14,15]. Among different nanomaterials, silver nanoparticles (AgNPs) have been well-established as one of the most effective agents for colorimetric probes because of their intense surface plasmon resonance (SPR) bands, high molar extinction coefficients, and extreme sensitivity to

environment perturbations. These features render AgNPs promising utilities for colorimetric sensing purposes [16,17].Sustainable methods have emerged as the main concern in the synthesis of AgNPs. Green synthesis is an attractive method in which biological molecules, such as amino acid derivatives, as reducing and stabilizing agents. Given its straightforwardness, ease of the reactions and the biocompatible nanoparticles, this method has received increasing attention [18]. The green synthesis is advantageous over conventional chemical and physical techniques, as it does not utilize toxic substances and harsh reaction conditions that are harmful to the environment and human health. Cost-effective, scalable and size- and shape-controlled synthesis of nanoparticles is necessary for a range of medical and drug detection applications[19,20] .This study aimed to synthesize, develop, and optimize a colorimetric assay for the detection of methamphetamine. Using a colorimetric aptasensing method is based on silver nanoparticles (AgNPs), which are characterized by a strong Local surface plasmon resonance (LSPR), resulting in strong colour changes upon aggregation.

2. Experimental

2.1. Chemicals

Silver nitrate ($AgNO_3$) from Merck chemicals (Germany), N-Acetyl-L-Cysteine, NaCl and phosphate buffered saline from Sigma-Aldrich (USA), KOH from WVT (Belgium), ethanol and methanol from Scharlau (Spain), cellulose dialysis membrane from HIMEDIA (India), methamphetamine was obtained from Basrah Forensic Office (Iraq), The 40-mer aptamer (5'-ACGTTTGCAATGTGGATGGTGTGGTATATGTGGTATTTGG-3') from Macrogen (South Korea).

2.2. Green Synthesis of Silver Nanoparticles

Different concentrations of $AgNO_3$ (3, 6, 8, 10, 15, and 20 mM, 9 mL) were gradually added to a solution of NAC (50 mM, 1 mL) and KOH (50 mM, 1 mL) at 100℃ with stirring. After 1 min, the mixture reaction turned brown from colorless. For more bio-reduction, the reaction was further stirred at 100℃ for 1 h, as shown in Fig. 1. The purification process was carried out using a cellulose rinsed membrane to remove the access of KOH, $AgNO_3$ and free N-acetyl-L-cysteine molecules, if any. The solutions were then rinsed using deionized water for 48 h. After washing, the samples were centrifuged at 3000 rpm (30 minutes) and rinsed two times with distilled water. This step was followed by a second centrifugation for 15 min to obtain further purification of the samples. Next, the samples were washed 3 times with ethanol (5 mL), and centrifuged for another 15 min. The emulsions obtained were finally dried under vacuum to yield high quality silver nanoparticles.

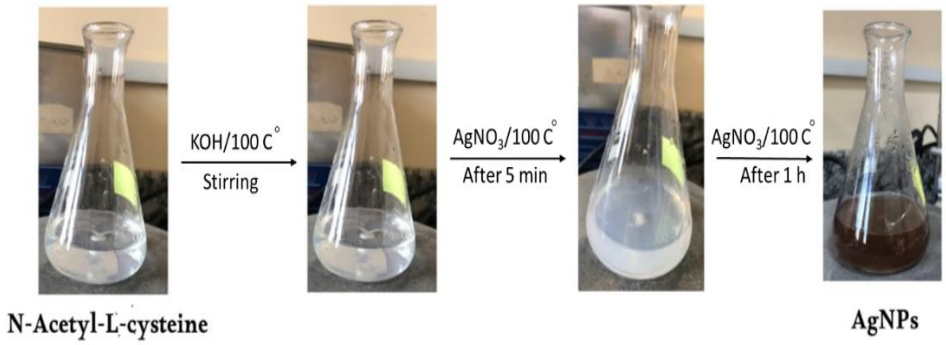

Figure 1. Schematic illustration for the biosynthesis steps of AgNPs

2.3. Characterizations of silver nanoparticles

N-Acetyl-L-Cysteine-AgNPs produced via green method have been defined by spectroscopic techniques that included UV–visible spectroscopy (Shimadzu UV-1800). Fourier transform infrared spectroscopy (FTIR) (4000–400 cm^{-1}) (Shimadzu FTIR 8400S), and /X-ray diffraction (PHILIPS, PW1730) with an operating voltage of 30 kV and a current of 40 mA, with Cu-Kα radiation (λ= 0.1540 nm). The samples were observed under a transmission electron microscope (TEM, Din Petronic Company, Zeiss). The chemical composition of green-synthesized silver nanoparticles was investigated with a FE-SEM/EDX (Day Petronic Company, Zeiss). Note: For clarity, the particle size analyzers: Brookhaven 90 plus for DLS and the HORIBA SZ-100 for Z-potentials.

2.5. Colorimetric biosensor of methamphetamine

All reactions for AgNPs sensing assay were performed in Eppendorf vial. In the first step, 100 µL of 10 nM AgNPs in distilled water was introduced to each vial. Subsequently, 10 µL of 1 µM methamphetamine-aptamer (dissolved in Nucleus distilled water) was supplemented. The mixture was incubated at 45 min for the binding of aptamer with nanoparticles. After incubation, 120 µL of methamphetamine (METH) at different concentrations (0, 10, 15, 20, 25, 30, 35, and 40 µM) were added to the separate vials, and then 10 µL of 250 mM NaCl solution was added to initiate the nanoparticle aggregation [21,22]. Color changes were visually monitored: the development of a yellow or brown color indicated a positive result (presence of METH) [23], whereas a colorless solution indicated a negative result.

3. RESULTS AND DISCUSSIONS

The first step of detecting a synthesized nanoparticle is visually observing its color [24]. the color changed from colorless to reddish brown. For making different concentrations of AgNPs, silver nanoparticles were synthesized using various amounts of silver nitrate ($AgNO_3$) at concentrations of 3, 6, 8, 10, and 15 mM. (Figure 2).

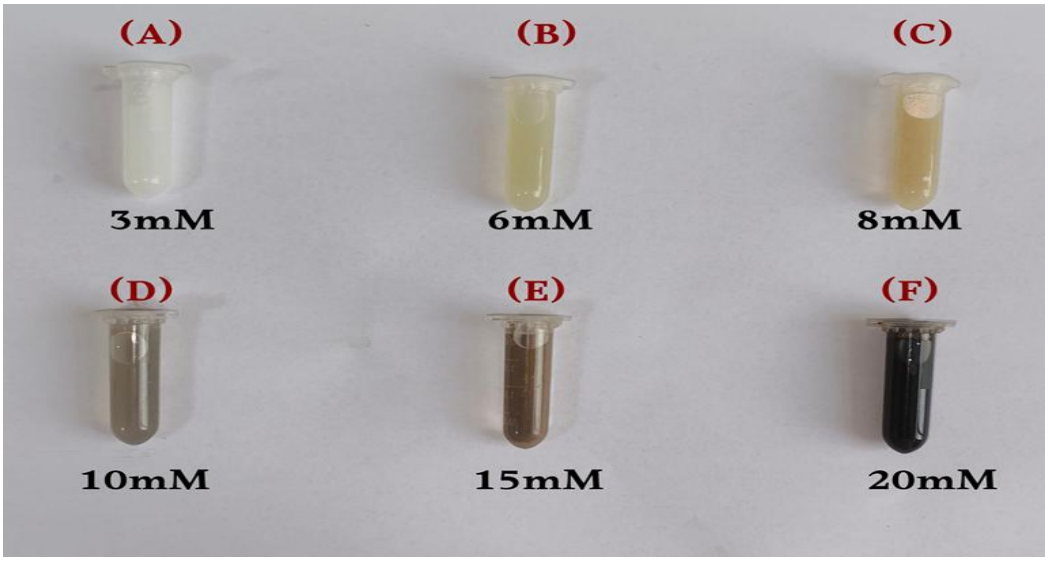

Figure 2. Different colors of silver nanoparticles prepared at different concentrations of $AgNO_3$

3.1. UV–Visible Spectrophotometric analysis

Pure silver nanoparticles generally feature absorption peaks at wavelengths above 390 nm [25]. If the absorption occurs at wavelengths shorter than this window, may have some impurities, solvent residues, or some other chemical in the sample. The formation of AgNPs is revealed by Local Surface Plasmon Resonance (LSPR) d -the interaction between electromagnetic radiation and metal nanoparticles resulting in coherent oscillations [26]. The synthesis involved preparing AgNPs with various levels of silver nitrate ($AgNO_3$) concentrations (3, 6, 8, 10, and 15) mM. Wavelength was then analyzed for all these concentrated derivatives as shown in Figure 3. There is no peak wavelength for these concentrations indicating a similar manner in that they have not had any silver nanoparticles. The UV-visible absorption spectroscopy at 20 mM concentration of the prepared silver nanoparticle colloidal solution by the N-Acetyl-L-cysteine showed that the synthesized silver nanoparticles exhibited a characteristic absorption peak at around 410 nm, which demonstrated that the biosynthesis of AgNPs was completed successfully. The presence of localized surface Plasmon resonance (LSPR) not only leads to high luminous efficiency but also stability against mechanical evaluation [27].

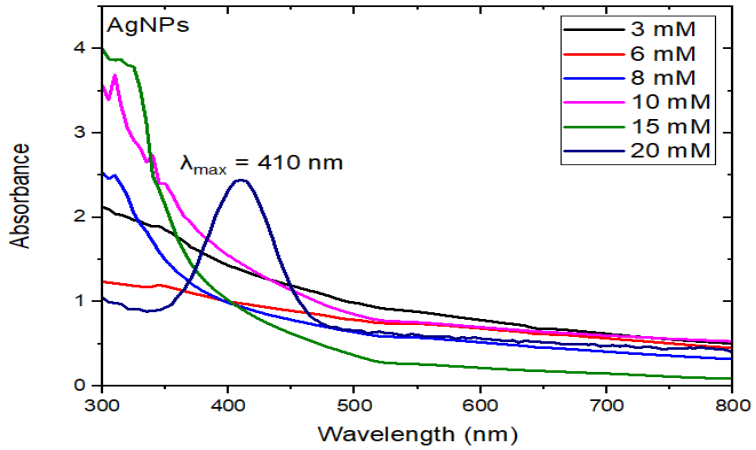

Figure3. UV-VIS maximum absorbance for the silver nanoparticles (AgNPs) prepared from different concentrations of $AgNO_3$

3.2. Functional Organic Group FTIR analysis

Figure 4A and B show the FTIR spectra of pure N-Acetyl-L-cysteine (NAC) and the silver nanoparticles synthesized using NAC as both a reducing and capping agent, respectively. The spectrum in Fig.4A displays the characteristic absorption bands of NAC [28], whereas Figure 4B illustrates the spectral changes that occur upon nanoparticle formation due to interactions between NAC and the silver surface. A wide absorption in the NAC spectrum at 3368 cm^{-1} could be assigned to O–H and/or N–H stretching vibrations. This band undergoes a positive shift (3320 cm^{-1}) in the nanoparticle spectrum, which is explicit proof of the participation of these functional groups in capping. The C–H stretching vibrations (2986 cm^{-1}, 2938 cm^{-1}) are not affected, suggesting minimal interaction in this region. The band at 2543 cm^{-1} in the NAC spectrum is assigned to the thiol (–SH) group and its absence in the silver nanoparticle spectrum indicates that the thiol group is attached to the silver and is involved in the synthesis of silver nanoparticles. The position of the C=O (amide) stretching vibration at 1708 cm^{-1} in the NAC spectrum and its slight shift to 1694 cm^{-1} upon nanoparticle formation also confirms the attachment of the amide with the nanoparticle surface.

International Journal of Environmental Sciences
ISSN: 2229-7359
Vol. 11 No. 11s, 2025
https://theaspd.com/index.php

Additional well-defined alterations are noted in the COO^- asymmetric and symmetric stretching peaks which move from 1527 cm^{-1} and 1410 cm^{-1} in NAC to 1518 cm^{-1}, 1463 cm^{-1}, and 1379 cm^{-1} in the nanoparticle spectrum. The changes indicate the involvement of the carboxylate group in stabilization. Moreover, the C–N/C–O and C–O stretching vibrations shift to higher frequencies due to changes in the chemical environment by the attachment on the silver substrate.

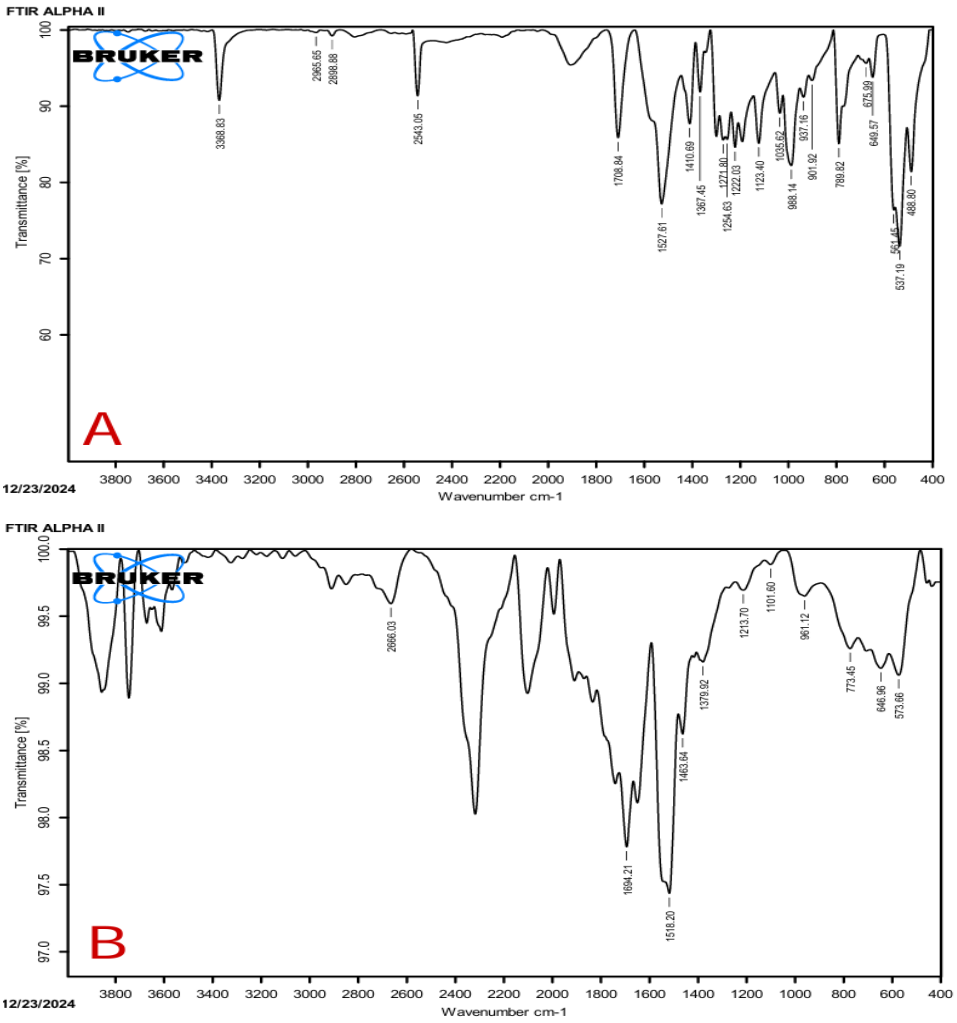

Figure 4. FTIR spectra analysis of (A) N-Acetyl-L-Cysteine (B) N-Acetyl-L-Cysteine- AgNPs

3.3. X-Ray Diffraction analysis

The crystal structure and phase composition of the prepared AgNPs were determined by X-ray diffraction (XRD) analysis. The XRD pattern shows distinct and sharp peaks which are indicative of the crystallinity and nanocrystalline nature of the silver nanoparticles. The intense Bragg reflections were recorded at about 38.29°, 44.07°, 60.07° and 64.78° of 2θ values; which can be indexed to the (111), (200), (220) and (311) powder crystallographic planes, respectively (Dhar et al., 2021). These peaks of metallic Ag are attributed to the face-centered cubic (FCC) structure and accord well with the standard reference data (JCPDS card no. 00-004-0783). Among these, the (111) reflection was the most intense, indicating a preferred orientation along this crystallographic plane. The existence of well-defined peaks in the XRD pattern indicates the

crystalline nature of the AgNPs, whereas the weak background can be associated with the amorphous molecule (NAC) of the capping or stabilizing agent as a by-product of synthesis [29] , as shown in Fig.5. The size of the nanoparticles was determined using the Scherrer equation considering the Full Width at Half Maximum (FWHM) of the most intense diffraction peaks. The calculated crystallite sizes are listed in Table 1. The crystal sizes are found to be varied from approximately 15.48 - 47.32 nm with an average crystal size of 28.47 nm. These results proved that the synthesis approach leads to well-crystallized nanosized silver particles, which are promising for catalysis, biosensing, and biomedicine processes as they are highly crystalline at the nanometer-sized level .

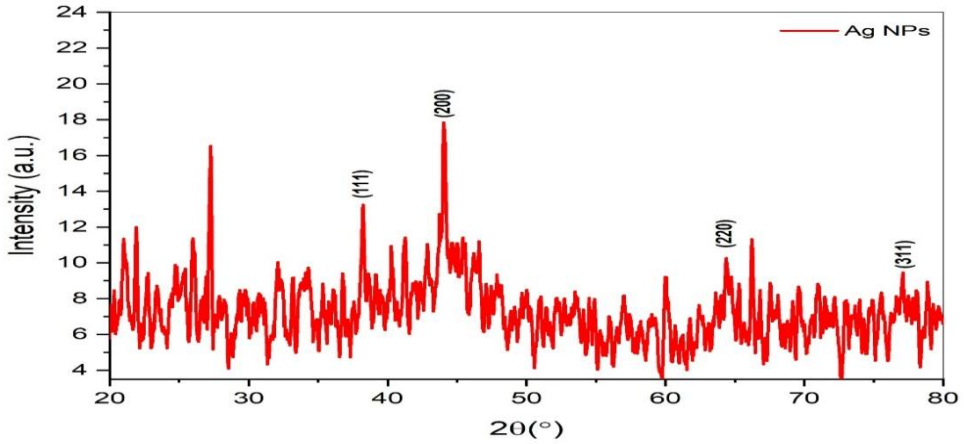

Fig.5. X-ray diffraction pattern of N-acetyl-L-cysteine-AgNPs

Table 1. XRD data and crystallite size of silver nanoparticles.

2 theta (deg.)	hkl	FWHM (deg.)	2 theta (Rad.)	FWHM (Rad.)	D (nm)	Matched by
38.28771	111	0.543168	0.334	0.009	15.476	00-004-0783
44.07209	200	0.181056	0.385	0.003	47.317	
60.06665	220	0.271584	0.524	0.005	33.775	
64.77667	311	0.543168	0.565	0.009	17.313	
Mean Particle Size					**28.470**	

3.4. Transmission Electron Microscopy (TEM)

The morphology, size and distribution of the formed silver nanoparticles (AgNPs) induced by N-Acetyl-L-cysteine (NAC) were also elucidated utilizing TEM (micrograph in Figure 6A). For TEM sample preparation, a drop of the colloidal solution of AgNPs was placed on a copper grid covered with carbon and dried at room temperature. The imaging was conducted at an accelerating voltage of 20.00 kV, using a STEM II detection mode at a magnification of 1,000,000× as noted in the micrograph metadata. The TEM image evidently confirms that the fabricated AgNPs are reasonably monodispersed and are predominantly of spherical shape. The nanoparticles seem to be isolated, suggesting good stabilization, probably caused by the capping of the NAC molecules. The boundaries of the particles become quite smooth and pronounced, and very little sign of agglomeration is observed [30]. For selected particles, some nanoparticles were directly measured from the TEM image with sizes varying nearly from 7.4 to 12.9 nm. This local measurement helps to understand single

nanoparticle size but for statistical validation, the complete profile of the nanoparticle population was studied by analyzing the particle size distribution (by ImageJ software). Thus the particle size distribution analysis (histogram Figure 6B) indicates that the range is from about 10 nm to 50 nm. The most frequent size of particles is between 15 and 25 nm, which are unimodal distributed. The data were fit to a Gaussian distribution curve, and the average particle size was estimated to be ~22.79 nm. This disagreement between individual TEM values and the mean is due to both the intrinsic sampling variation and the fact that only a limited number of particles are tagged for direct measurement in the micrograph. However, it was proved that the NAC-assisted synthesis route effectively synthesizes nano-silver of uniform morphology and nanometric size appropriate for bio-catalyst applications.

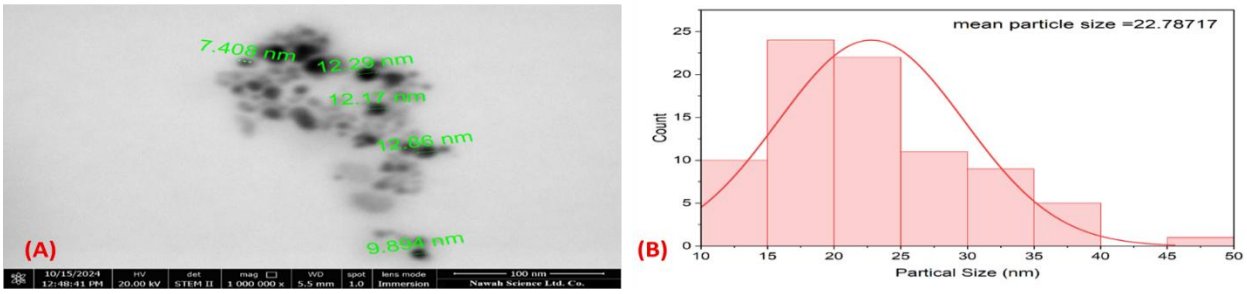

Figure 6. (A) TEM image of NAC –AgNPs (B) size distribution of AgNPs and average diameter

3.5. Field Emission Scanning Electron Microscopy (FE-SEM) and Energy-Dispersive X-Ray Spectroscopy (EDX) Analysis

From the SEM images, the shape, size and distribution of nanoparticles could be analyzed [31]. In FESEM, the high electric field of the radiations drives the electrons into the sample. The sample surface is irradiated with this concentrated electron beam, which results in the production of secondary electrons. These secondary electrons are detected in order to reconstruct the surface profile of the sample with high fidelity. The Scanning Electron Microscope (SEM) detects backscattered electrons ejected from the surface of a sample under test. The silver nanoparticles (AgNPs) are used for SEM study, because of their electrical conductivity. One advantage of SEM is the ability to examine samples on a dark background (few scattering). Although SEM is useful for assessing the purity of the NPs and agglomeration, it does not offer structural information [32]. AgNPs are commonly found in various shapes such as oval, spherical, triangular, pebble, cubic, and rod. While Transmission Electron Microscopy (TEM) provides only 2D images, SEM may provide additional three-dimensional (3D) details about the morphology of nanoparticles [33] The surface structure of the synthesized silver nanoparticles (AgNPs), which were synthesized via the N-Acetyl-L-cysteine reduction and stabilization method, is depicted in Figure 7. The structure is an aggregation, but the individual particles are almost spherical and were very uniformly distributed. SEM micrograph of the particles with a magnification of 350,000×. These nanoparticles seem to be in nanometer size, well-aggregated to very crowded aggregates with a moderate uniform size distribution. Based on the morphology of these shapes achieved, a successful reduction and stabilization process is presumed, which presumably owes to the thiol and amine groups of N-Acetyl-L-cysteine capable of chelating with metal ions and suppressing uncontrolled agglomeration. The absence of large or nonspherical particles is another evidence of the high yield and control of the synthetic process.

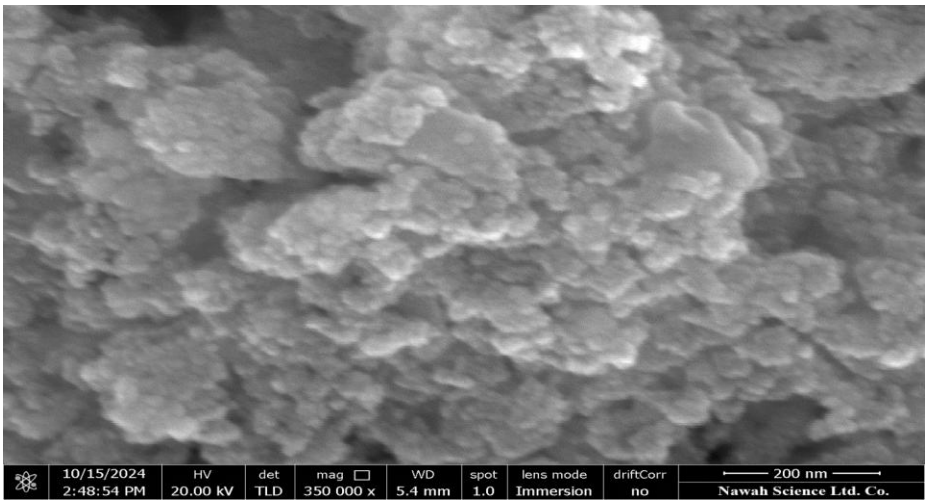

Figure 7. FE-SEM Micrograph of NAC-AgNPs

In electron microscopy, X-rays emitted from the sample are detected using the Energy-Dispersive X-ray Spectroscopy (EDX) technique. The EDX detector analyzes the intensity and energy of the emitted X-rays to assess their relative abundance [34]. Furthermore, EDX is utilized to identify both the qualitative and quantitative elemental composition of nanomaterials [35].The atomic composition of the prepared material was verified by EDX analysis (Figure 8). The EDX spectrum shows one major peak the silver (Ag) at about 70.15 wt%, suggesting the high purity and as-grew of silver nanoparticles. In addition to silver, large intensity peaks were observed for oxygen (16.80 wt%) and sulfur (7.31 wt%). This sulfur may originate from the thiol (-SH) group of N-Acetyl-L-cysteine showing its participation in surface functionalization and stabilization of the nanoparticles. Such oxygen can be due to surface oxidation or originate from hydroxyl or carboxyl groups on the capping agents. Small amounts of chlorine (0.89 wt%) and gold (0.15 wt%) were also found, gold is probably from the substrate or the sample holder. In general, the EDX analysis provides evidence for the successful synthesis and functionalization of silver nanoparticles in the presence of N-Acetyl-L-cysteine.

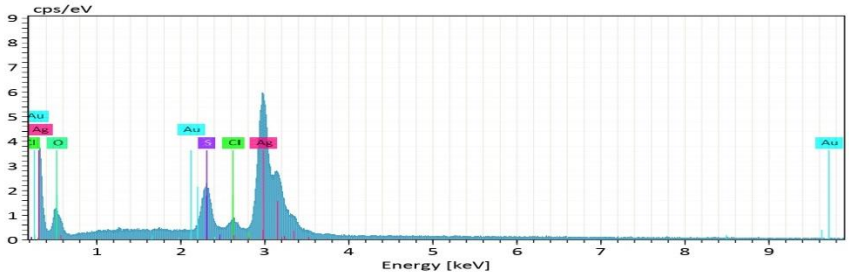

Figure 8. Elemental analysis of NAC-AgNPs by EDX

3.6. Dynamic Light Scattering (DLS) and Z-Potential Analysis

Dynamic Light Scattering (DLS) is a commonly used technique in particle size measurement as its analysis time is short and the equipment required is not very expensive as compared to some other techniques [36]. The principle is that of the determination of hydrodynamic size, which is taken as that of an equivalent hard sphere that diffuses at the same rate as the species of interest within the DLS instrument [37]. DLS analysis was employed to monitor the particle size of the prepared AgNPs, indicating that N-Acetyl-L-cysteine was an effective reducer and stabilizer for the production of NAC-AgNPs (Figure 9). DLS analysis revealed that the

total average particle size of AgNPs is around 51.95 nm. The relatively homogeneous dispersion of the nanoparticles was confirmed by the particle size distribution, which showed a moderate uniformity (PDI = 0.378).

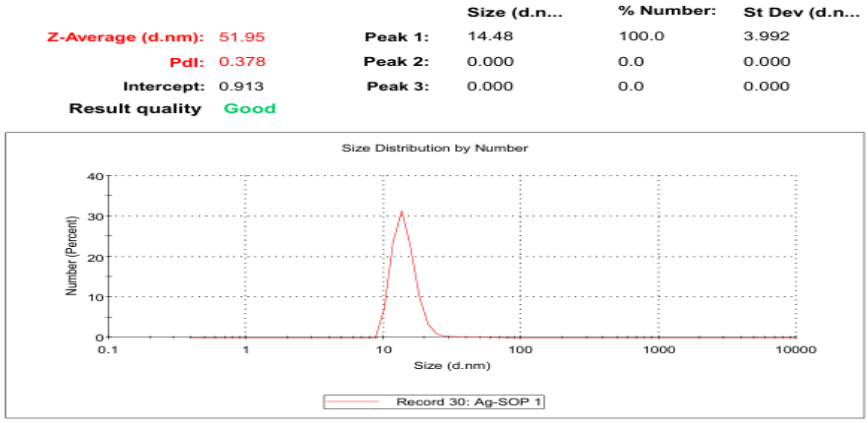

Figure 9. Dynamic light scattering of NAC -AgNPs

The stability of biosynthesized nanoparticles was determined by the Zeta potential of the nanoparticles as the surface charge. The zeta potential measurement confirmed the stable existence of the nanoparticles in colloidal suspension. This is in agreement with the general guideline that a Zeta potential value greater than +30 mV or less than -30 mV is necessary for the colloidal stability of nanoparticles [38]. The synthesized silver nanoparticles exhibited a negative surface charge, indicating good colloidal stability [39] . Zeta potential analysis revealed a value of -29.2 mV for the NAC-AgNPs, suggesting that the particles are near the threshold of electrostatic stability in colloidal suspension Figure 10.

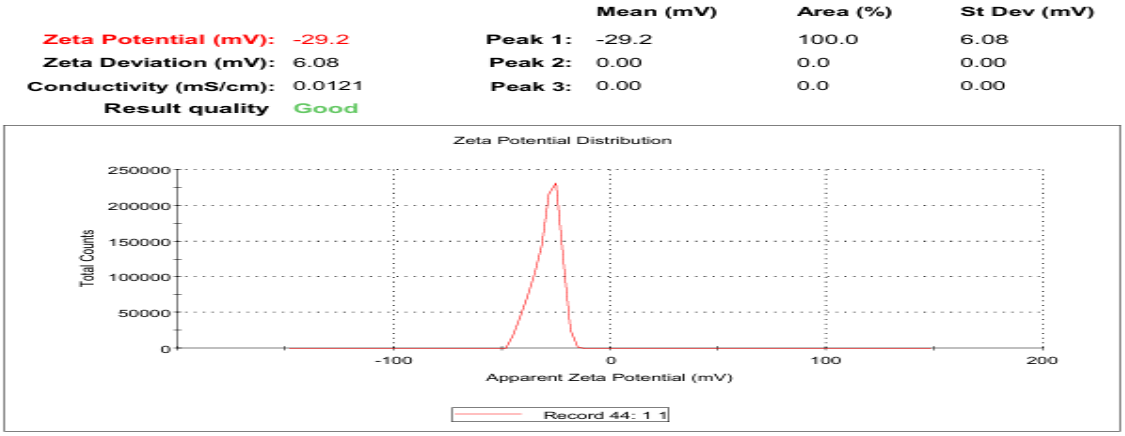

Figure 10. Zeta-potential analysis of NAC -AgNPs

2.7. Silver Nanoparticles-Aptamer Biosensor

One of the common platforms for colorimetric aptasensing is based on silver nanoparticles (AgNPs). These particles are characterized by a strong surface plasmon resonance (SPR), which results in strong color (yellow for AgNPs) changing upon aggregation [40]. In the absence of methamphetamine, aptamers act as a stabilizing agent for the nanoparticle itself and prevent the nanoparticles from agglomeration. Nevertheless, in the case that the aptamer is bound with methamphetamine, these aggregates are formed to cause a noticeable color change (colorless to yellow for AgNPs) as shown in Figure 11 [41,42].

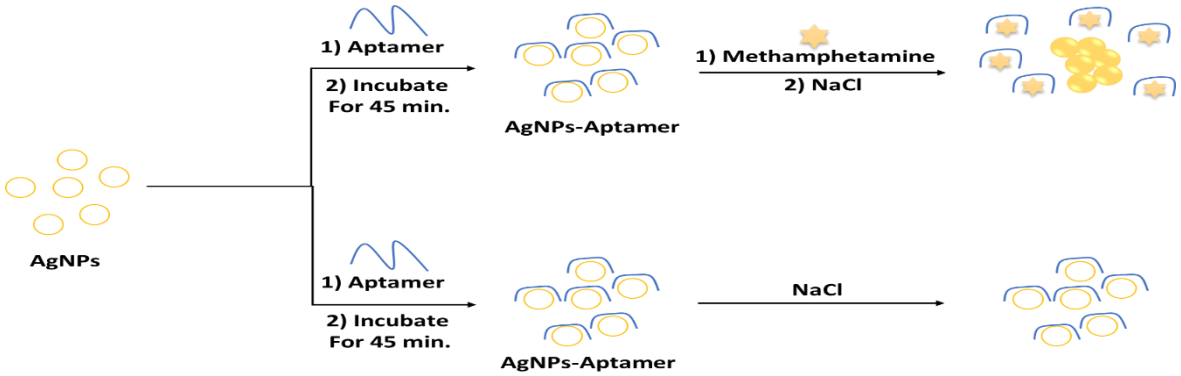

Figure 11. Schematic Illustration of the Aptamer-Based Colorimetric Biosensor using Silver Nanoparticles

To elucidate the mechanism of detection, control experiments were performed, and the corresponding UV-Vis spectra are shown in Figure 12. The AgNPs combined with the aptamer alone showed a characteristic absorbance peak at ~410 nm, indicating nanoparticle stability. The addition of NaCl to AgNPs without the aptamer induced partial aggregation, as shown by a broadened peak with a slight red shift. In contrast, the AgNP-aptamer-NaCl system (in the absence of METH) exhibited suppressed aggregation, confirming the aptamer's protective effect [43] . However, upon the addition of METH to the AgNP-aptamer-NaCl system, aggregation was substantially increased, which is manifested by enhanced absorbance at 554 nm and decreased absorbance at 410 nm. This indicated that the methamphetamine could compete with methamphetamine aptamer to bind with AgNP, which could make the aptamer leave the surface of the presence of the salt-induced aggregation [44].

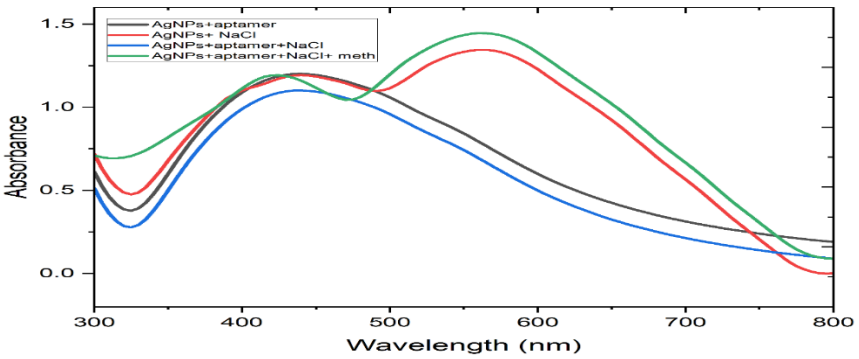

Figure 12. Comparative UV-Vis Spectra Showing the Role of Each Component in the AgNP–Aptamer Biosensor System

3.7.1. Optimization of experimental conditions

In order to obtain the optimum condition for the METH detection, A series of experiments with different NaCl concentrations was performed to examine the effect of ionic strength on AgNP stability. A constant concentration of AgNPs (10 nM) was mixed with increased amounts of NaCl (0-500 mM) [45]. The aggregation status of AgNPs was determined by monitoring UV–Vis spectrophotometric profiles with a focus on absorbance 410 nm and 554 nm which are characteristic of surface plasmon resonance (SPR) of dispersed and aggregated AgNPs, respectively (Figure 13A). At low salt (≤50 mM), low A_{554}/A_{410} ratios suggest few aggregates and good dispersion of AgNPs. However, the ratio increases sharply once the NaCl concentration exceeds 100 mM, indicating a considerable shift to aggregated species. The ratio maximizes at around 250

mM and then becomes constant, suggesting a saturation of the aggregation. For practical applications, particularly if AgNP stability or monitoring the aggregation is the goal (i.e. there is a target in mind, such as sensing or catalysis), these findings are crucial. Then, it is assumed that 250 mM NaCl is the best concentration for achieving pronounced and reliable AgNPs aggregation under the studied conditions.

A time-dependent experiment was performed in order to confirm the incubation time at which the aptamer and AgNPs can be most effectively conjugated. Aptamer at a final concentration of 1 μM was incubated with 10 nM of AgNPs at different time points (5, 15, 30, 45, 60, 90 and 120 min). Subsequently, the aggregation of AgNPs was observed by UV–Vis spectroscopy where the absorbance at 410 and 554 was measured, and the aggregation index was expressed as the ratio. The increase in aggregation ratio was larger during the first 45 min of the incubation (Figure 13B), suggesting that aptamer binding to the AgNP surface became significantly tight. The most significant increase was observed between 15 and 45 minutes, with the ratio rising from approximately 0.25 to 1.38. This indicates that the adsorption of aptamers on the surface of AgNP is kinetic and is a gradual process over this time [46].

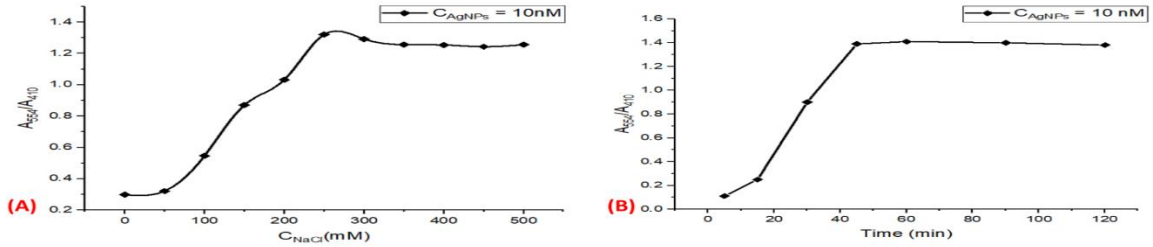

Figure 13. (A) NaCl concentration-dependent change in the absorbance intensity ratio (A_{554}/A_{410}) of AgNPs solution. (B) Incubation time-dependent change in the absorbance intensity ratio (A_{554}/A_{410}) of the AgNPs–aptamer solution

3.7.2. Detection of METH

A colorimetric assay for methamphetamine (METH) was constructed using label-free silver nanoparticles (AgNPs) modified with methamphetamine-targeted aptamer. The detection strategy was based on salt-induced aggregation of AgNPs upon introduction with (or without) METH, which resulted in a different colorimetric/spectrophotometric variation [47]. The development of the Eppendorf tube's color was observed as a function in concentrations of METH (0–40 μM) as shown in Figure 14. The solution was virtually color-free at 0 μM, with a slight change in coloration at 10 μM; however, as the concentration of METH was raised, the yellow-brown coloration became more intense, which directly corresponds to successful detection of METH by aggregation of the nanoparticles.

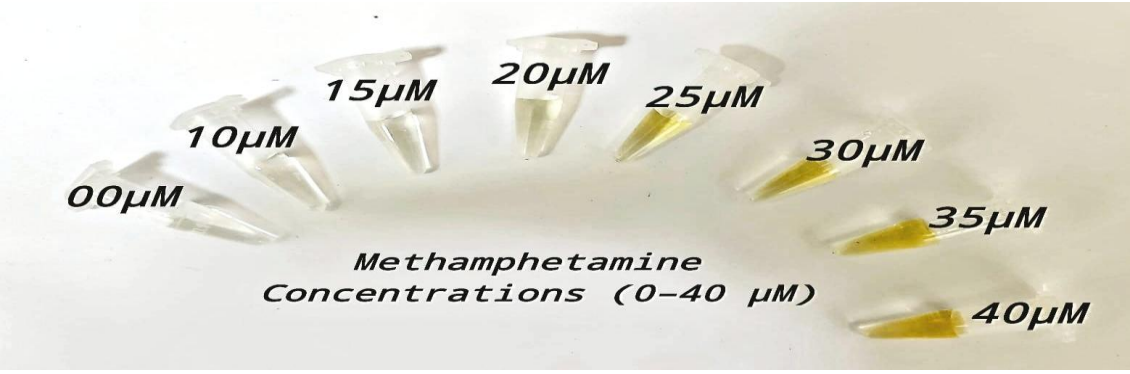

Figure 14. Visual colorimetric response of the AgNP–Aptamer biosensor to increasing methamphetamine concentrations (0–40 μM)

For further evidencing the visual observations, the change of absorbance as a result of different METH concentrations was investigated using UV-Vis spectroscopy. The absorptions against a reference of samples with 0 to 40 μM METH are shown in Figure 15. Two typical peaks can be seen at about 410 nm for the dispersed AgNPs and about 554 nm for the aggregated NPs. The intensity of the 410 nm peak was lowered and its red shift with the intensity increased of the 554 nm peak as the concentration of METH increased. Such spectral characteristic, therefore corroborates increased nanoparticle aggregations at a higher concentration of METH that is in line with the visual images. The spectral shift was especially remarkable above 20 μM indicating a threshold for discrimination.

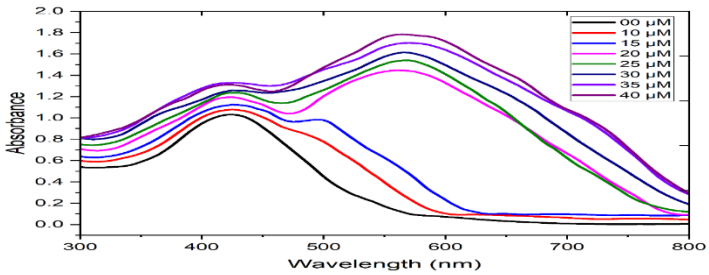

Figure 15. UV-Vis Absorbance Spectra of the AgNP–Aptamer Biosensor at Varying Methamphetamine Concentrations

The response time of the AgNPs-aptamer biosensor for detecting METH was determined by spectrophotometrically monitoring the colorimetric change with time post addition of METH (25 μM) and NaCl. The absorbance ratio, a parameter indicating the aggregation condition of AgNPs, was monitored at several time points shown in Figure 16. The data obviously showed that the ratio of absorbance had a quick rise during the first 2 min, reflecting the fast aggregation of AgNPs by the binding of METH to the aptamer in the presence of NaCl. Following this early rapid rise, the absorbance ratio leveled off, indicating the aggregation reaction was completed and reached equilibrium soon thereafter. This rapid colorimetric behavior validates the high efficiency and fast response kinetics of the biosensor system, which can meet the need of timely detecting METH in practical use.

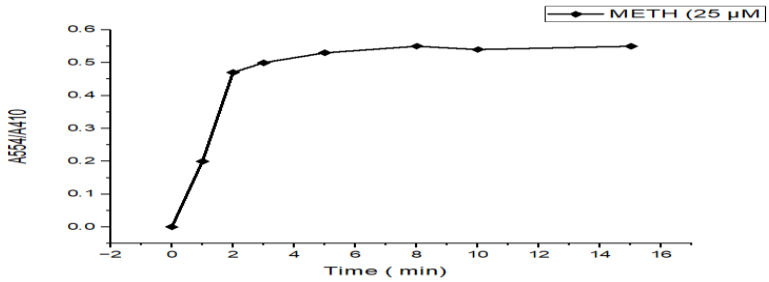

Figure 16. Time-dependent variation in the absorbance ratio of the AgNPs-aptamer biosensor after the addition of METH (25 μM) and NaCl

4. CONCLUSION

In conclusion, this study demonstrates a greener, easier and more reproducible approach to the preparation of AgNPs with N-acetyl-L-cysteine. The AgNPs obtained upon the addition of a methamphetamine-specific aptamer were developed into an ultrasensitive colorimetric biosensor for detecting METH. Characterization verified the good properties of the nanoparticles and the sensor showed high sensitivity, selectivity, and

responsive rate. With visible appearance and qualitative verification with a UV-Vis spectrophotometer. These results demonstrate the potential of the biosensor as a simple, low-cost, and user-friendly diagnostic tool to detect drugs, particularly under resource-limited settings and point-of-care applications.

REFERENCES

1. Jayanthi, S., Daiwile, A. P. & Cadet, J. L. Neurotoxicity of methamphetamine: Main effects and mechanisms. *Exp Neurol* 344, 1–29 (2021).
2. Harro, J. Neuropsychiatric adverse effects of amphetamine and methamphetamine. in *International Review of Neurobiology* vol. 120 179–204 (Academic Press Inc., 2015).
3. Jayanthi, S., Daiwile, A. P. & Cadet, J. L. Neurotoxicity of methamphetamine: Main effects and mechanisms. *Exp Neurol* 344, 1–12 (2021).
4. Shrestha, P. *et al.* Methamphetamine induced neurotoxic diseases, molecular mechanism, and current treatment strategies. *Biomedicine and Pharmacotherapy* vol. 154 1–18 Preprint at https://doi.org/10.1016/j.biopha.2022.113591 (2022).
5. Ben-Yehuda, O. & Siecke, N. Crystal Methamphetamine: A Drug and Cardiovascular Epidemic ∗. *JACC: Heart Failure* vol. 6 219–221 Preprint at https://doi.org/10.1016/j.jchf.2018.01.004 (2018).
6. Cohen-Laroque, J. *et al.* Positive and negative symptoms in methamphetamine-induced psychosis compared to schizophrenia: A systematic review and meta-analysis. *Schizophrenia Research* vol. 267 182–190 Preprint at https://doi.org/10.1016/j.schres.2024.03.037 (2024).
7. Al-Imam, A. *et al.* Risk Factors of Suicidal Ideation in Iraqi Crystal Methamphetamine Users. *Brain Sci* 13, 1–19 (2023).
8. Al-Imam, A. & Michalak, M. Iraq's Meth Crisis: Prioritizing Research to Combat Suicidal Ideation. *Al-Kindy College Medical Journal* vol. 20 78–79 Preprint at https://doi.org/10.47723/f2m0tp28 (2024).
9. Wang, W. *et al.* Exploring the mechanism of trait depression and cognitive impairment on the formation of among individuals with methamphetamine use disorder under varying degrees of social support. *Front Public Health* 13, 1–10 (2025).
10. Riahifar, V., Haghnazari, N., Keshavarzi, F. & Ahmadi, E. A sensitive voltammetric sensor for methamphetamine determination based on modified glassy carbon electrode using Fe3O4@poly pyrrole core-shell and graphene oxide. *Microchemical Journal* 170, 1 (2021).
11. Orfanidis, A. *et al.* A GC–MS method for the detection and quantitation of ten major drugs of abuse in human hair samples. *J Chromatogr B Analyt Technol Biomed Life Sci* 1047, 141–150 (2017).
12. Koichi Saito, M. T. Y. Y. R. I. Analysis of Methamphetamine in Urine by HPLC with Solid-Phase Dispersive Extraction and Solid-Phase Fluorescence Derivatization. *Chem. pharm. Bull.* 71, 24–30 (2023).
13. Concheiro, M. *et al.* Fast LC-MS/MS method for the determination of amphetamine, methamphetamine, MDA, MDMA, MDEA, MBDB and PMA in urine. *Forensic Sci Int* 171, 44–51 (2007).
14. Xu, Y. *et al.* Colorimetric detection of kanamycin based on analyte-protected silver nanoparticles and aptamer-selective sensing mechanism. *Anal Chim Acta* 891, 298–303 (2015).
15. Xu, Y. *et al.* Colorimetric detection of kanamycin based on analyte-protected silver nanoparticles and aptamer-selective sensing mechanism. *Anal Chim Acta* 891, 298–303 (2015).
16. Loiseau, A. *et al.* Silver-based plasmonic nanoparticles for and their use in biosensing. *Biosensors* vol. 9 1–39 Preprint at https://doi.org/10.3390/bios9020078 (2019).
17. Bidan, A. K. & Al-Ali, Z. S. A. Biomedical Evaluation of Biosynthesized Silver Nanoparticles by Jasminum Sambac (L.) Aiton Against Breast Cancer Cell Line, and Both Bacterial Strains Colonies. *Int J Nanosci* 21, (2022).
18. Al-Majeed, S. H. A., Al-Ali, Z. S. A. & Turki, A. A. Biomedical Assessment of Silver Nanoparticles Derived from L-Aspartic Acid Against Breast Cancer Cell Lines and Bacteria Strains. *Bionanoscience* 13, 1833–1848 (2023).
19. Kadhim, A. S. & Al-Ali, Z. S. A. Green Synthesis of Reduced Graphene Oxide Nanosheets using Iraqi Rhus coriaria (L.) Fruits Extract and a Study of Its Anticancer Activity. *Iraqi Journal of Science* 65, 6253–6266 (2024).
20. Bidan, A. K. & Al-Ali, Z. S. A. Oleic and Palmitic Acids with Bioderivatives Essential Oils Synthesized of Spherical Gold Nanoparticles and Its Anti-Human Breast Carcinoma MCF-7 In Vitro Examination. *Bionanoscience* 13, 2293–2306 (2023).
21. Shi, Q. *et al.* Colorimetric and bare eye determination of urinary methylamphetamine based on the use of aptamers and the salt-induced aggregation of unmodified gold nanoparticles. *Microchimica Acta* 182, 505–511 (2015).
22. Alfadly, A., Abdulwahid, A. & Saleh, A. Fast colorimetric method for the detection of captagon based on a general sensor design involving aptamers and gold nanoparticles. *Nano Biomed Eng* 12, 124–131 (2020).

23. Endo, T., Ikeda, R., Yanagida, Y. & Hatsuzawa, T. Stimuli-responsive hydrogel-silver nanoparticles composite for development of localized surface plasmon resonance-based optical biosensor. *Anal Chim Acta* 611, 205–211 (2008).
24. Essghaier, B. *et al.* Biosynthesis and Characterization of Silver Nanoparticles from the Extremophile Plant Aeonium haworthii and Their Antioxidant, Antimicrobial and Anti-Diabetic Capacities. *Nanomaterials* 13, 1–17 (2023).
25. Albert, H. M. *et al.* Biosynthesis, Spectroscopic, and Antibacterial Investigations of Silver Nanoparticles. *J Fluoresc* 1, 1–11 (2023).
26. Lin, G. *et al.* A Surface-Enhanced Raman Scattering Substrate with Tunable Localized Surface Plasmon Resonance Absorption Based on AgNPs. *Sensors* 24, 1–11 (2024).
27. Alzoubi, F. Y., Ahmad, A. A., Aljarrah, I. A., Migdadi, A. B. & Al-Bataineh, Q. M. Localize surface plasmon resonance of silver nanoparticles using Mie theory. *Journal of Materials Science: Materials in Electronics* 34, 1–10 (2023).
28. Koleva, B., Spiteller, M. & Kolev, T. Polarized spectroscopic elucidation of N-acetyl-l-cysteine, l-cysteine, l-cystine, l-ascorbic acid and a tool for their determination in solid mixtures. *Amino Acids* 38, 295–304 (2010).
29. Vishwajeet, S., Ankita, S. & Nitin, W. Biosynthesis of silver nanoparticles by plants crude extracts and their characterization using UV, XRD, TEM and EDX. *Afr J Biotechnol* 14, 2554–2567 (2015).
30. Said, A., Abu-Elghait, M., Atta, H. M. & Salem, S. S. Antibacterial Activity of Green Synthesized Silver Nanoparticles Using Lawsonia inermis Against Common Pathogens from Urinary Tract Infection. *Appl Biochem Biotechnol* 196, 85–98 (2024).
31. Thiurunavukkarau, R. *et al.* Silver nanoparticles synthesized from the seaweed Sargassum polycystum and screening for their biological potential. *Sci Rep* 12, 1–11 (2022).
32. Barabadi, H. *et al.* Green synthesis, characterization, antibacterial and biofilm inhibitory activity of silver nanoparticles compared to commercial silver nanoparticles. *Inorg Chem Commun* 129, 1–10 (2021).
33. Helmlinger, J. *et al.* On the Crystallography of Silver Nanoparticles with Different Shapes. *Cryst Growth Des* 16, 3677–3687 (2016).
34. Bamal, D. *et al.* Silver nanoparticles biosynthesis, characterization, antimicrobial activities, applications, cytotoxicity and safety issues: An updated review. *Nanomaterials* vol. 11 1–40 Preprint at https://doi.org/10.3390/nano11082086 (2021).
35. Alomar, T. S. *et al.* Designing Green Synthesis-Based Silver Nanoparticles for Antimicrobial Theranostics and Cancer Invasion Prevention. *Int J Nanomedicine* 19, 4451–4464 (2024).
36. Dogiparthi, L. K. *et al.* Phytochemical mediated synthesis of silver nanoparticles and their antibacterial activity. *SN Appl Sci* 3, 1–8 (2021).
37. Iwuji, C. *et al.* Synthesis and characterization of silver nanoparticles and their promising antimicrobial effects. *Chemical Physics Impact* 9, 1–6 (2024).
38. Baran, A. *et al.* Ecofriendly/Rapid Synthesis of Silver Nanoparticles Using Extract of Waste Parts of Artichoke (Cynara scolymus L.) and Evaluation of their Cytotoxic and Antibacterial Activities. *J Nanomater* 2021, 1–10 (2021).
39. Patil, R. B. & Chougale, A. D. Analytical methods for the identification and characterization of silver nanoparticles: A brief review. in *Materials Today: Proceedings* vol. 47 1–13 (Elsevier Ltd, 2021).
40. Amendola, V. Surface plasmon resonance of silver and gold nanoparticles in proximity of graphene studied with the discrete dipole approximation method. *Journal: Physical Chemistry Chemical Physics* 1, 1–25 (2015).
41. Yarbakht, M. & Nikkhah, M. Unmodified gold nanoparticles as a colorimetric probe for visual methamphetamine detection. *J Exp Nanosci* 11, 593–601 (2016).
42. Endo, T., Ikeda, R., Yanagida, Y. & Hatsuzawa, T. Stimuli-responsive hydrogel-silver nanoparticles composite for development of localized surface plasmon resonance-based optical biosensor. *Anal Chim Acta* 611, 205–211 (2008).
43. Mao, K. *et al.* A novel colorimetric biosensor based on non-aggregated Au@Ag core–shell nanoparticles for methamphetamine and cocaine detection. *Talanta* 175, 338–346 (2017).
44. Anzar, N. *et al.* Paper-Based Electrodes Decorated with Silver and Zinc Oxide Nanocomposite for Electro-Chemical Sensing of Methamphetamine. *Sensors* 23, 1–13 (2023).
45. Lodeiro, P., Achterberg, E. P., Pampín, J., Affatati, A. & El-Shahawi, M. S. Silver nanoparticles coated with natural polysaccharides as models to study AgNP aggregation kinetics using UV-Visible spectrophotometry upon discharge in complex environments. *Science of the Total Environment* 539, 7–16 (2016).
46. Zhao, J. *et al.* Enhancement of radiosensitization by silver nanoparticles functionalized with polyethylene glycol and aptamer As1411 for glioma irradiation therapy. *Int J Nanomedicine* 14, 9483–9496 (2019).
47. Roushani, M. & Shahdost-Fard, F. A novel ultrasensitive aptasensor based on silver nanoparticles measured via enhanced voltammetric response of electrochemical reduction of riboflavin as redox probe for cocaine detection. *Sens Actuators B Chem* 207, 764–771 (2015).